Nanoscale

Cite this: *Nanoscale*, 2012, **4**, 6279

www.rsc.org/nanoscale

COMMUNICATION

Graphene nanoribbon-guided fluid channel: a fast transporter of nanofluids

Ling Liu,*[a] Lin Zhang,[a] Zhongguo Sun[b] and Guang Xi[b]

Received 13th July 2012, Accepted 13th August 2012
DOI: 10.1039/c2nr31847d

In this work, we present a conceptual design of nanofluid channels using graphene sheets as the container and nanoribbons as flow guiders. Using molecular dynamics simulations, we demonstrate that water molecules confined in such nanochannels can be well guided by the nanoribbons and form a regular shaped water stream. The viscosity of water transported along such nanochannels is found to be orders of magnitude lower than that of bulk water. Several unconventional structural and flow characteristics are revealed to be responsible for the fast transport phenomenon comparable to that in carbon nanotubes. The proposed nanoribbon-guided fluid channel is promising for use in next-generation integrated material systems for transporting fluids at high volumetric flow rates with considerably low driving forces.

Nanoconfined fluids have attracted enormous attention in the past decade due to the continuous development of novel nanoporous and low-dimensional materials and the increasing demand for extraordinary physical and chemical properties that are not achievable in conventional fluids. Confined in nanopores with sizes ranging from sub-nanometer to a few nanometers, most ions and molecules in nanofluids can be considered as being in close contact with the confining solid atoms. The interfacial interferences, along with the intrinsic size effects at the nanoscale, strongly perturb the physical and chemical properties of nanofluids, which has led to many unconventional and sometimes even counterintuitive behaviors of nanofluids. For instance, the transport viscosity of water confined in carbon nanotubes (CNTs) was found to be orders of magnitude lower than that of the bulk water.[1] As a result, fast transport of fluids in CNTs has been observed,[2,3] with flow rates comparable to that in biological channels such as aquaporins.[4] For electrolytes confined in nanocavities, ionic solubility[5] and hydration[6] are both reduced, which strongly affect the ionic infiltration[7] and diffusion,[8] making nanofluid behavior specific to ions.[9] Nanofluid behavior is also very sensitive to the local chemical and physical environments. With the appropriate design of nanocavity sizes and functional groups anchored to solid atoms, many nanoporous materials have been designed for separating phases from their mixtures and forming nanopatterned mixtures of multiple phases *via* self-assembly. Examples include dehydration of ethanol,[10] capturing CO_2 from a gas mixture,[11–13] desalination of seawater,[14,15] gas trapping[16] for phase separation, and the spontaneous formation of semimicelle and fractal-like micelle of surfactants in tunable CNTs for self-assembled nanopatterning.[17] Due to these superior properties and intriguing behaviors, nanofluids have emerged as an important source for engineering innovations to advance the technologies of energy absorption,[18,19] actuation,[20,21] and energy and environmental sustainability,[12–15] among others.

Many materials can provide nanocavities to accommodate fluid phases, including natural materials like zeolites and silica, biological materials like the various ion channels, synthetic nanoporous materials like metal-organic-frameworks (MOFs)[22] and covalent-organic-frameworks (COFs),[23] and synthetic low-dimensional materials like CNTs[24] and boron nitride nanotubes (BNTs).[25] Among them, CNT-confined nanofluids are considered advantageous for many applications and have been subjected to extensive investigation. This is due to the many attributes of CNTs that can significantly enhance the desired properties of nanofluids confined in them. For example, the simple composition of CNT provides a highly stable accommodation; the ultra-smooth surface permits ultra-fast transport of confined nanofluids; and moreover, thanks to the development of many advanced synthesis techniques, the size and topology as well as the surface chemistry of CNTs are highly tunable, which not only provides opportunities for new applications but also helps to optimize the results.

In addition to CNTs, graphene nanoribbon is another type of low-dimensional materials that has aroused considerable interest in recent years.[26,27] A large volume of research has been devoted to the exploration and understanding of their remarkable mechanical, thermal and electronic properties,[28,29] but the nanofluidics associated with nanoribbons is relatively underexplored. Previous studies have mainly focused on hydrophobic interactions in nanoconfinements formed by nanoribbons[30,31] and the induced nucleation of nanobubbles.[30] However, ongoing efforts to produce micro-patterned nanoribbons on graphene sheets[32] have shed inspiring light on the use of nanoribbons for flexible device applications, including many of those based on nanofluidics. It is, therefore, of great interest to explore the possibility of utilizing nanoribbons in mediating nanofluid flows, and to study the associated chemical and physical properties of nanofluids.

Here, we propose a conceptual nanoribbon-guided fluid channel (NRC) as illustrated in Fig. 1. The fluid phase is sandwiched in between two monolayer graphene sheets, on each of which a nanoribbon is attached to shape a pathway for conducting nanofluid flow.

[a]*Department of Mechanical and Aerospace Engineering, Utah State University, Logan, UT 84322, USA. E-mail: ling.liu@usu.edu*
[b]*School of Energy and Power Engineering, Xi'an Jiaotong University, Xi'an, Shanxi 710049, China.*

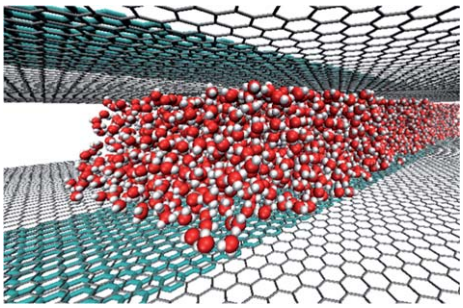

Fig. 1 Illustration of a graphene nanoribbon-guided nanofluid channel (NRC): a flow of water molecules is confined in a straight nanochannel shaped by two nanoribbons transferred atop two graphene sheets that are in direct contact with the water molecules.

As such, a layered composite nanofluid system is created in the order of "nanoribbon-graphene-fluid-graphene-nanoribbon". In this design, graphene sheets are introduced to contain vapors, and the nanoribbons are incorporated to serve as "guiders" for mediating the nanofluid flow.

In order to understand the performance of the proposed NRC, a representative-cell model is built for four NRCs as shown in Fig. 2a. The four NRCs are modeled to have the same length of 213 Å (along the z-direction). The distances between all neighboring nanoribbon and graphene layers are 3.35 Å (along the y-direction). The widths of all nanoribbons (along the x-direction) are 36 Å. All graphene layers are modeled wide enough to eliminate the edge effects. The only variable among the four NRCs is the separation between the two graphene sheets, denoted by h. "NRCh" is therefore employed to denote the different cases, with h = 15 Å, 20 Å, 25 Å, and 30 Å, respectively. The periodic boundary condition is applied only in the z-direction to ensure the continuity of the flow. Due to different h values, 1190, 2940, 4900, and 6300, water molecules are confined in NRC15, NRC20, NRC25, and NRC30, respectively. For simplicity, the graphene sheets and nanoribbons are constrained and all water molecules are made movable.

A systematic study is then conducted to explore the static (equilibrium) and dynamic (transport) behaviors of water confined in NRCs, which includes a systematic quantification of density, dipole moment, hydrogen bonding, transport viscosity (size- and velocity-dependent), along with detailed flow characteristics, under various conditions. All these quantities selected for investigation are important characterizations of fluid behaviors in nanoconfinements. In particular, viscosity as a measure of flow resistance serves as a critical indicator of the efficiency of a nanochannel for transporting nanofluids. In the equilibrium analysis, the confined water phase is made stationary. In the transport analysis, however, water molecules are loaded to induce a pressurized flow with a center-of-mass velocity, v, along the z-direction. The transport analysis includes two parts: (1) steady-state transport, in which v is maintained a constant, and (2) decelerated transport, in which the driving force is removed in the middle of a steady-state transport so that the liquid phase is freely decelerated from a non-zero initial velocity. Note that in steady-state transport analysis, driving forces of different magnitudes can drive the confined nanofluid to flow at different velocities, which enables us to investigate the role of flow velocity in the transport phenomena.

Molecular dynamics (MD) is adopted in this work using LAMMPS[33] as the computational platform. Water molecules are modeled by the TIP3P model.[34] The particle–particle particle–mesh method (PPPM) is used to address the long range Coulomb interactions with a root mean square accuracy of 10^{-4}.[35] The room temperature of 300 K is maintained by applying the Nosé–Hoover thermostat. The temperature calculation subtracts the center-of-mass velocity, v, of the water flow in the transport analysis. All simulations are performed for a sufficiently long duration to obtain sound statistical results of key descriptors of the confined nanofluid behaviors. Note that, in the simulations of steady-state transport, it usually takes several nanoseconds for the flow to reach the steady-state (*i.e.* constant v with reasonable thermal fluctuations), so only outputs in the steady-state regime are used for analysis.

For the equilibrium analysis, by averaging the positions of particles over time, point-wise mass density of water can be obtained in the unit kg m^{-3}. By analyzing the statistical distribution of the dipole moment orientation in a specific region, the preferential alignment of water molecules is obtained. A similar approach is also applied to evaluate the spatial variation of hydrogen bonding between water molecules. Two water molecules are considered to be hydrogen bonded if (1) the O–O distance is below 3.5 Å, and (2) the angle between the O–O axis and an O–H bond is smaller than 30°.[36] However, for the transport analysis, point-wise velocity vectors can be obtained in the unit of m s^{-1} by time-averaging the velocities of

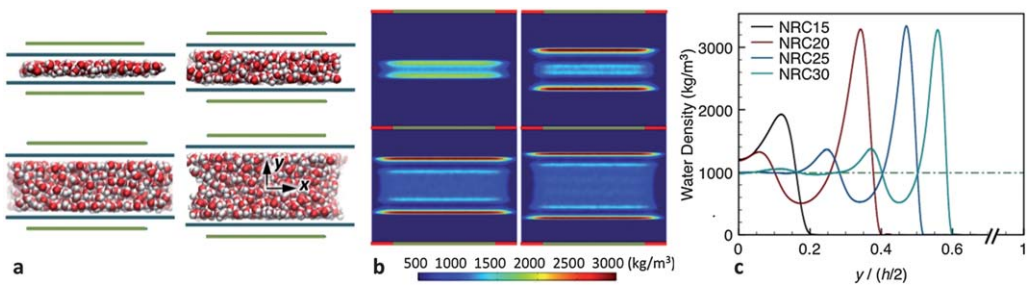

Fig. 2 Four model NRCs are considered with the separation between opposite graphene sheets, h, equal to 15 Å, 20 Å, 25 Å, and 30 Å, respectively. They are denoted as NRCh (h = 15, 20, 25 and 30). (a) Cross-sectional view of the water-filled NRCs. Blue lines indicate the vertical positions of the graphene sheets, and green lines depict nanoribbons. An x–y coordinate system is shown with z defined perpendicular to the x–y plane. (b) Contours of point-wise water density within the NRCs. The charts are scaled in the y direction by h so that the top and bottom edges (red lines) all correspond to the vertical positions of the graphene sheets. The green lines in between red lines indicate the width of the nanoribbons. (c) Point-wise water density along the thickness direction (y-axis). Only $y > 0$ is shown because of the symmetry of the system about the x-axis. The vertical coordinate, y, is normalized by $h/2$, such that the right edge of the plot ($y/(h/2) = 1$) corresponds to the position of the top graphene sheet.

water molecules appearing in the region. Each of the velocity vectors can be further decomposed into two components: the axial velocity along the flow direction, v_z, and the velocity projected onto the cross-sectional plane, v_{x-y}. Averaging the axial velocities of all water molecules gives the center-of-mass velocity, v. The deceleration, shearing stress, and viscosity are then evaluated.

Different from CNTs and many other nanochannels in which nanofluids are confined by "visible" geometric boundaries of the solids, NRCs guide nanofluid flow *via* an "invisible" force field exerted by the nanoribbons. From an atomic point of view, as a fluid molecule (or ion) is confined in an NRC, its balance is controlled by three factors: forces exerted by other fluid molecules (and ions), interaction with the graphene layers, and interaction with the nanoribbons. Considering the edge effects of the nanoribbons, the most energetically favorable position for the confined fluid phase must be centered about the perpendicular bisector of the nanoribbons (y-axis). This is verified by Fig. 2a, in which four snapshots depicting the equilibrated water phase confined in NRCs are illustrated. In all cases, water is found to reside in the center of the NRCs and occupies a straight flow pathway shaped by the nanoribbons. The same phenomenon is also observed in Fig. 2b, in which contours of water density are plotted. Apparently, all contours are symmetric about the y-axis, implying that the confined water is equilibrated in the center of the NRCs. Both graphs serve as direct demonstrations of the fact that even without any geometric constraint along the width direction (x-direction), NRCs can still attract fluids and center them in the nanochannel. As will be shown below, this unique characteristic, together with other attributes of NRCs, induces ultra-fast transport of water with significantly low viscosities.

Fig. 2b also suggests a layered structure for water confined in NRCs. In all cases, water is found to be significantly densified in the first layer of water molecules from the solid surface (also called the first solvation shell, FSS). According to Fig. 2c that plots the variation of water density along the y-axis, the peak density in NRC15 is found to be about 2000 kg m^{-3}, two times that of bulk water; in the other cases, even higher peak densities are identified (approximately 3200 kg m^{-3}). Theoretically, comparing fluid molecules (or ions) at interfaces and those in the bulk, the former are subjected to more complicated force fields, so their equilibrium positions must be different from those in the bulk. Such interfacial effects are especially critical for nanofluids, in which almost all molecules (and ions) are in close contact with the confining solid atoms. As such, nanofluids confined in NRCs are unevenly distributed, which is coupled with many other unique properties and intriguing behaviors of nanofluids.

In addition to the uneven distribution of density, some other descriptors of NRC-confined water are also spatially varied, such as the orientation of dipole moment, which quantifies the alignment of water molecules (Fig. 3a), and the hydrogen bonding, an attractive interaction between water molecules that is critical for determining water properties such as boiling and surface tension. Fig. 3b plots the statistical distribution of the dipole moment orientation, θ, in three selected NRCs at two representative positions, FSS and MID. FSS refers to the first solvation shell, while MID refers to the center of the NRC. In NRC15, FSS and MID are equivalent, as there exists only one layer of concentrated water due to the extreme confinement. According to Fig. 3b, in the FSS of NRC15, the dipole moment orientation is unevenly distributed. The water molecules seem to prefer $\theta = 90°$ and 270° to other angles, implying that dipole moments parallel to the solid surface are more energetically favored.

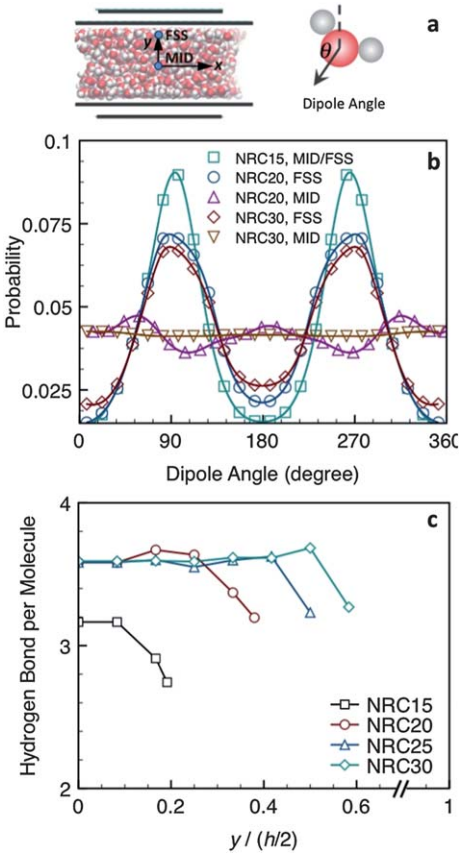

Fig. 3 (a) In-plane orientation of the water dipole moment, θ, is defined as the angle between the y-axis and the in-plane component of the dipole vector as illustrated by the arrow. (b) Probability distribution of the in-plane dipole moment orientation at two representative vertical positions, *i.e.* FSS and MID as defined in (a). FSS refers to the first solvation shell and MID is in about the center of the NRC. (c) Number of hydrogen bonds per water molecule *versus* vertical position.

By comparing NRC20 and NRC30, a similar distribution is noted in the FSS but the distributions in MID are found to be distinct. In the NRC30 of a larger confinement, MID is far away from the solid surface so the interfacial effect is much diminished; dipole moments in this region thus have equal probability to face different directions, similar to that in bulk water. In NRC20, however, the interfacial effect still remains to some extent, although it is already very close to a flat distribution. In contrast, Fig. 3c plots the number of hydrogen bonds per molecule, n_{HB}, along the thickness direction. In all cases, n_{HB} is found to drop rapidly in the FSS from a constant of about 3.6. This is partly due to the densification of water molecules in the FSS that has a free surface, and also partly due to the preferential alignment of dipole moment with the solid surface. After all, hydrogen bonding is defined by both the separation and angle between two water molecules,[36] so both local density and dipole moment distribution can influence its formation.

Previous research has demonstrated that nanofluid transport can be ultra-fast in CNTs[2,3] because of the smoothness of the solid surfaces,[37] low viscosity of the confined nanofluids,[1] and a thermodynamically driven depletion layer at interfaces.[38,39] With the same chemical composition and similarly simple geometries, NRCs are expected to have comparable performance. In addition, NRCs also

have an apparent advantage over CNTs. With the tunable width (or cross-sectional area), NRCs can transport a larger volume of nanofluids than CNTs, and the volumetric flow rate can be easily adjusted by changing the width of the nanoribbons.

The transport characteristics of a nanochannel can be quantified by three quantities, *i.e.* the deceleration of a fluid column freely transporting inside the nanochannel, a, the shearing stress exerted by the solid surface, τ, and the viscosity of the nanoconfined fluid phase, η. These three quantities are closely correlated. a (as measured by the free deceleration test, inset of Fig. 4a) quantifies the per-molecule flow impedance. From the mechanics point of view, the deceleration is caused by the lattice resistance of the solid to the fluid flow, which is quantified by the shearing stress, τ. τ can be correlated with a *via* $\tau = \rho_L m_0 a/2w$ where ρ_L denotes the line number density which is equal to the number of water molecules in a unit length of the nanochannel, m_0 is the mass per water molecule, and w is the width of the nanoribbons. The viscosity, η, can be determined by $Q = h^3 w\Delta P/12\eta L$, where Q denotes the flow rate, and ΔP is the pressure drop over the length of L. In addition, the equilibrium of the liquid column gives $wh\Delta P/L = 2\tau w$ and $Q = vwh$ where v denotes the flow velocity. Finally, a simple relationship is obtained between τ and η in the form of $\eta = \tau h/6v$.

Fig. 4a–c plots the deceleration, shearing stress, viscosity for water confined in the four model NRCs. All of these quantities are found to strongly depend on the size of the NRC and the velocity of the nanofluid flow. In small NRCs such as NRC15, all water molecules reside in the FSS and are in direct contact with the solid surface, so the flow impedance caused by the lattice resistance is peaked. With the size of NRC increased, more water molecules are subjected to low or negligible interactions with the solid surface, thus decreasing the flow impedance (Fig. 4a). Another important factor is the flow velocity. As the confined nanofluid is transported at a high velocity, the water molecules residing in the boundary layers are given less time to respond to the relative motion of atoms in the solid lattice, among other dynamically changing local environment variables. Hence, at high v, it is less likely that the interfacial water molecules adjust to the most energetically favorable positions, thus increasing the flow impedance (Fig. 4a).

Different from the deceleration that quantifies the per-molecule flow impedance, shearing stress quantifies the overall interaction between solid surfaces and confined nanofluids. From Fig. 2c, it is known that there are two shells of concentrated water in most of the NRCs except the smallest one under investigation, NRC15. The two shells, FSS and SSS (second solvation shell) are subjected to the strongest interactions with the solid atoms, which determine the shearing stress. Due to the similar interactions of FSS and SSS with solid surfaces in most reasonably large NRCs, the shearing stress in these NRCs should be almost the same. As shown in Fig. 4b, τ of NRC25 and NRC30 are found almost identical. Due to the relatively smaller confinement, τ of NRC20 is a little bit smaller but it is very close to that of the larger NRCs. τ of NRC15, however, is a lot smaller because only FSS exists and interacts with the solid surface. Like the velocity effect on a, shearing stress also increases with the flow velocity due to similar reasons.

As an intrinsic property of fluids, viscosity measures the resistance of fluids to the deformation caused by shearing stress or tensile stress. Due to the layered structure in NRCs, the viscosity of nanofluids is subjected to very prominent size effects. Water confined in NRC15 is shown to have the lowest viscosity (Fig. 4c), implying that the deformation of nanofluids can be assisted by larger free surfaces in smaller NRCs. As the size of NRC increases, η keeps increasing, but for all the four cases under investigation, the viscosity is about 3–4 orders of magnitude lower than that of bulk water. Fig. 4d–f plots a, τ, and η for water transported in four selected CNTs with the diameters equal to 8.12 Å, 13.56 Å, 27.12 Å, and 40.68 Å, respectively. They are denoted by CNT8, CNT14, CNT27, and CNT41, respectively, consistent with the notation of the NRCs. By comparing Fig. 4d–f with Fig. 4a–c, the computed viscosities all show prominent size and velocity effects; moreover, the absolute values of viscosity are found to be very comparable in both types of nanochannels. The

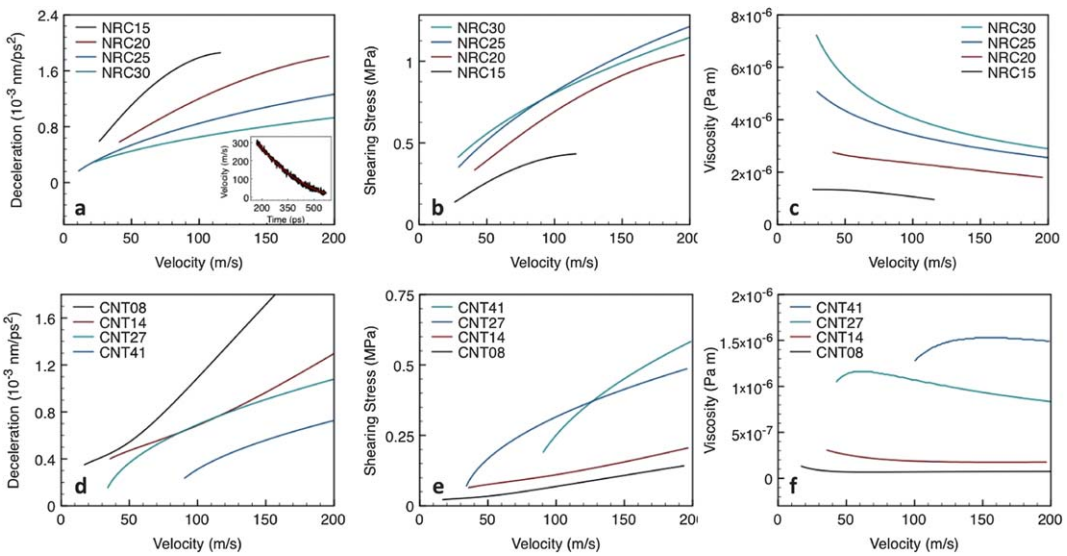

Fig. 4 Velocity-dependent (a) deceleration, (b) shearing stress, and (c) nominal viscosity of water confined in the four model NRCs. Inset of (a) plots the decreasing velocity *versus* time during the freely decelerated transport of water in NRC30. (d–f) Corresponding nanofluid descriptors in four representative carbon nanotubes (CNTs). The carbon nanotubes are armchair with the diameters equal to 8.12 Å (CNT08), 13.56 Å (CNT14), 27.12 Å (CNT27), and 40.68 Å (CNT41), respectively.

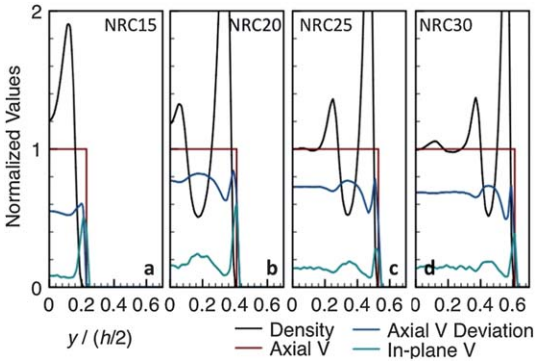

Fig. 5 Normalized density profile, axial velocity profile, standard deviation of axial velocity, and in-plane velocity profile along the *y*-direction (thickness direction, vertical) for the steady-state transport of water through four NRCs at 50 m s^{-1}. Density is normalized by the bulk water density, 1000 kg m^{-3}. All velocity-related variables are normalized by the axial flow velocity, *v*.

differences can be attributed to several factors including the curvature of CNTs, the additional nanoribbon layers in NRCs that are also in close interaction with the nanofluids, and the fact that no geometric constraint exists in NRCs along the width direction.

To further understand the flow of nanofluids along NRCs, a detailed analysis of the flow field is shown in Fig. 5. In addition to the well-known plug-like velocity profile and the depletion layer in which the axial velocity, v_z, suddenly drops, an interesting relationship between the density (ρ), in-plane velocity (v_{x-y}), and the standard deviation of v_z has also been found: regions with high ρ always have low v_{x-y} and small deviation of v_z, while those with low ρ always correspond to high v_{x-y} and large deviation of v_z. We suggest that in regions where water is diluted, water molecules have relatively higher mobility perpendicular to the flow direction, leading to more swaps with water molecules in other regions and thus larger deviation of v_z is identified. In regions with concentrated water, however, the space per molecule is quite limited, which significantly suppresses the in-plane activities of water molecules along with the swap mechanism.

To summarize, we have proposed a conceptual nanochannel using nanoribbons and graphene sheets to mediate nanofluid flows. Water confined in such nanochannels is found to be well guided by the nanoribbons and forms a regular shaped nanostream that has extremely low transport viscosities. The viscosity and other equilibrium and transport properties are found to strongly depend on the flow velocity and the size of the nanochannels. A new swap mechanism is revealed to be responsible for the nanofluid flows in NRCs. Different from slit pores,[40] the proposed NRCs employ nanoribbons as fluid guiders, which significantly increases the customizability and paves the road for manipulating nanofluids *via* nanoribbon networks. That thermal and electrical stimuli may serve as an additional way to control nanofluids to make the system highly responsive to multiple external fields deserves note.[20,21] Moreover, use of nanoribbons and graphene sheets in NRCs also permits the utilization of the remarkable mechanical, thermal, and electronic properties of these materials to create highly multifunctional systems.

Acknowledgements

This work is financially supported by Utah State University and the Space Dynamics Lab.

References

1 X. Chen, G. X. Cao, A. J. Han, V. K. Punyamurtula, L. Liu, P. J. Culligan, T. Kim and Y. Qiao, *Nano Lett.*, 2008, **8**, 2988–2992.
2 J. K. Holt, H. G. Park, Y. Wang, M. Stadermann, A. B. Artyukhin, C. P. Grigoropoulos, A. Noy and O. Bakajin, *Science*, 2006, **312**, 1034–1037.
3 M. Majumder, N. Chopra, R. Andrews and B. J. Hinds, *Nature*, 2005, **438**, 44.
4 P. Agre, *et al.*, in *Current Topics in Membranes*, Academic Press, 2001, vol. 51, pp. 1–38.
5 A. Malani, K. G. Ayappa and S. Murad, *Chem. Phys. Lett.*, 2006, **431**, 88–93.
6 Y. W. Tang, K. Y. Chan and I. Szalai, *Nano Lett.*, 2002, **3**, 217–221.
7 L. Liu, X. Chen, W. Y. Lu, A. J. Han and Y. Qiao, *Phys. Rev. Lett.*, 2009, **102**, 184501.
8 R. M. Lynden-Bell and J. C. Rasaiah, *J. Chem. Phys.*, 1996, **105**, 9266–9280.
9 D. J. Tobias and J. C. Hemminger, *Science*, 2008, **319**, 1197–1198.
10 Y. H. Wang, C. M. Gong, J. S. Sun, H. Gao, S. A. Zheng and S. M. Xu, *Bioresour. Technol.*, 2010, **101**, 6170–6176.
11 P. Nachtigall, M. R. Delgado, D. Nachtigallova and C. O. Arean, *Phys. Chem. Chem. Phys.*, 2012, **14**, 1552–1569.
12 J. D. Carruthers, M. A. Petruska, E. A. Sturm and S. M. Wilson, *Microporous Mesoporous Mater.*, 2012, **154**, 62–67.
13 J. An, S. J. Geib and N. L. Rosi, *J. Am. Chem. Soc.*, 2009, **132**, 38–39.
14 S. J. Kim, S. H. Ko, K. H. Kang and J. Han, *Nat. Nanotechnol.*, 2010, **5**, 297–301.
15 J. Yuan, X. Liu, O. Akbulut, J. Hu, S. L. Suib, J. Kong and F. Stellacci, *Nat. Nanotechnol.*, 2008, **3**, 332–336.
16 O. Hugon, M. Sauvan, P. Benech, C. Pijolat and F. Lefebvre, *Sens. Actuators, B*, 2000, **67**, 235–243.
17 N. Arai, K. Yasuoka and X. C. Zeng, *J. Am. Chem. Soc.*, 2008, **130**, 7916–7920.
18 Y. Qiao, L. Liu and X. Chen, *Nano Lett.*, 2009, **9**, 984–988.
19 F. B. Surani, X. Kong, D. B. Panchal and Y. Qiao, *Appl. Phys. Lett.*, 2005, **87**, 163111.
20 L. Liu, J. B. Zhao, P. J. Culligan, Y. Qiao and X. Chen, *Langmuir*, 2009, **25**, 11862–11868.
21 B. X. Xu, Y. Qiao, T. Park, M. Tak, Q. L. Zhou and X. Chen, *Energy Environ. Sci.*, 2011, **4**, 3632–3639.
22 H. Li, M. Eddaoudi, M. O'Keeffe and O. M. Yaghi, *Nature*, 1999, **402**, 276–279.
23 H. M. El-Kaderi, J. R. Hunt, J. L. Mendoza-Cortes, A. P. Cote, R. E. Taylor, M. O'Keeffe and O. M. Yaghi, *Science*, 2007, **316**, 268–272.
24 G. Hummer, J. C. Rasaiah and J. P. Noworyta, *Nature*, 2001, **414**, 188–190.
25 C. Y. Won and N. R. Aluru, *J. Am. Chem. Soc.*, 2007, **129**, 2748–2749.
26 X. Li, X. Wang, L. Zhang, S. Lee and H. Dai, *Science*, 2008, **319**, 1229–1232.
27 Y.-W. Son, M. L. Cohen and S. G. Louie, *Nature*, 2006, **444**, 347–349.
28 X. Jia, J. Campos-Delgado, M. Terrones, V. Meunier and M. S. Dresselhaus, *Nanoscale*, 2011, **3**, 86–95.
29 S. Dutta and S. K. Pati, *J. Mater. Chem.*, 2010, **20**, 8207–8223.
30 T. Koishi, *et al.*, *Phys. Rev. Lett.*, 2004, **93**, 185701.
31 S. Sharma and P. G. Debenedetti, *Proc. Natl. Acad. Sci. U. S. A.*, 2012, 4365–4370.
32 C. Jin, K. Suenaga and S. Iijima, *Nat. Nanotechnol.*, 2008, **3**, 17–21.
33 G. Meng, Y. J. Jung, A. Cao, R. Vajtai and P. M. Ajayan, *Proc. Natl. Acad. Sci. U. S. A.*, 2005, **102**, 7074–7078.
34 M. Terrones, H. Terrones, F. Banhart, J.-C. Charlier and P. M. Ajayan, *Science*, 2000, **288**, 1226–1229.
35 R. Hockney and J. Eastwood, *Computer Simulation Using Particles*, Taylor & Francis Inc., Bristol, PA, USA, 1981.
36 A. Luzar and D. Chandler, *Nature*, 1996, **379**, 55–57.
37 A. I. Skoulidas, D. M. Ackerman, J. K. Johnson and D. S. Sholl, *Phys. Rev. Lett.*, 2002, **89**, 185901.
38 A. Poynor, L. Hong, I. K. Robinson, S. Granick, Z. Zhang and P. A. Fenter, *Phys. Rev. Lett.*, 2006, **97**, 266101.
39 S. Joseph and N. R. Aluru, *Nano Lett.*, 2008, **8**, 452–458.
40 N. Gothard, C. Daraio, J. Gaillard, R. Zidan, S. Jin and A. M. Rao, *Nano Lett.*, 2004, **4**, 213–217.